JACS
JOURNAL OF THE AMERICAN CHEMICAL SOCIETY
pubs.acs.org/JACS
Article

Emissive Colloidal GaAs Quantum Dots

Jun Hyuk Chang, Danial Zangeneh, Heng-Chi Chu, Justin C. Ondry, Kailai Lin, Yuan Liu, Zirui Zhou, Ahhyun Jeong, James Cassidy, Sungsu Kang, Scott A. Crooker, Alexander S. Filatov, A. Paul Alivisatos, Eran Rabani, Robert F. Klie, Richard D. Schaller, Alexander L. Efros, and Dmitri V. Talapin*

Cite This: J. Am. Chem. Soc. 2026, 148, 22804−22816

Read Online

ACCESS | Metrics & More | Article Recommendations | Supporting Information

ABSTRACT: Colloidal quantum dots offer tunable optical properties for optoelectronic applications, but the synthesis of high-quality III−V quantum dots (QDs) other than indium pnictides, and particularly GaAs, has remained elusive due to synthetic challenges. Colloidal GaAs QDs have been reported very recently and have shown only weak band-edge photoluminescence. Here, we demonstrate a large-scale synthesis of colloidal GaAs QDs in molten salts, followed by a high-temperature surface treatment with K_2S, which removes native oxide and enables uniform zinc chalcogenide shell growth on GaAs. These QDs demonstrate bright band-edge photoluminescence and electroluminescence in QD LED devices. Low-temperature spectroscopy reveals a well-resolved exciton fine structure with distinct bright-state splitting and temperature-independent decay dynamics from 4 to 100 K. These results establish a practical pathway for the preparation of high-quality colloidal GaAs QDs from molten salts with potential applications in quantum technologies and optoelectronics.

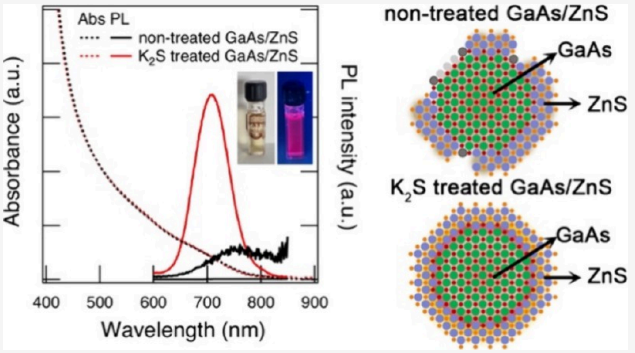

INTRODUCTION

Colloidal quantum dots (QDs) exhibit size-dependent optical and electronic properties,[1] enabling their use in a wide range of applications, including displays,[2] lasers,[3] luminescent solar concentrators,[4] photodetectors,[5] and solar cells.[6] The appeal of colloidal QDs arises from their scalable solution-based synthesis capable of producing uniform nanocrystals with controlled size, shape, and composition, which can be processed in different ways, such as inkjet printing or blending with polymers. Over the past two decades, cadmium chalcogenide[7,8] and indium pnictide[9−13] QDs have demonstrated outstanding optoelectronic properties, firmly establishing colloidal QDs as versatile materials for fundamental studies and real-world applications.

However, many thin-film semiconductors currently used in lighting,[14,15] laser diodes,[16] and photovoltaics[17] are based on Ga and Al containing III−V compounds, which are typically synthesized by high-temperature gas-phase processes such as molecular beam epitaxy (MBE) or metal−organic chemical vapor deposition (MOCVD). Epitaxially grown GaAs quantum dots in particular represent a benchmark for quantum emitters, exhibiting single-photon indistinguishability and subnanosecond radiative lifetimes.[18−20] Despite the materials' central role in modern optoelectronics, the development of high-quality colloidal Ga or Al containing III−V QDs has lagged considerably behind their thin-film counterparts.[21,22] This limitation has prevented Ga and Al containing III−V QDs from reaching their full potential in applications where their intrinsic properties, such as direct bandgaps, weak electron−phonon coupling, and high stability under heat and light stress, would be advantageous.

To address this challenge, our group has been developing molten inorganic salts as reaction media for dispersing,[23] modifying by cation-exchange,[24−28] and synthesizing[29] novel QDs at high temperatures required for materials with covalent bonds. This approach has already enabled the synthesis of band-edge emitting GaAs QDs, a breakthrough given GaAs's importance as one of the most studied III−V semiconductors and as a cornerstone material for high-speed transistors, solar cells, and lasers. Building upon this progress, we sought to determine whether large-scale synthesis applies to various optoelectronic applications and whether the optical properties of GaAs QDs could be further enhanced by shell growth. More specifically, we needed to address the important questions of whether molten salt-synthesized colloidal GaAs QDs could achieve the optical quality of epitaxial counterparts, whether standard surface passivation and shell growth strategies translated to this materials system, and how their excitonic

Received: February 13, 2026
Revised: April 27, 2026
Accepted: May 4, 2026
Published: May 29, 2026

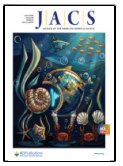

https://doi.org/10.1021/jacs.6c03474
J. Am. Chem. Soc. 2026, 148, 22804−22816

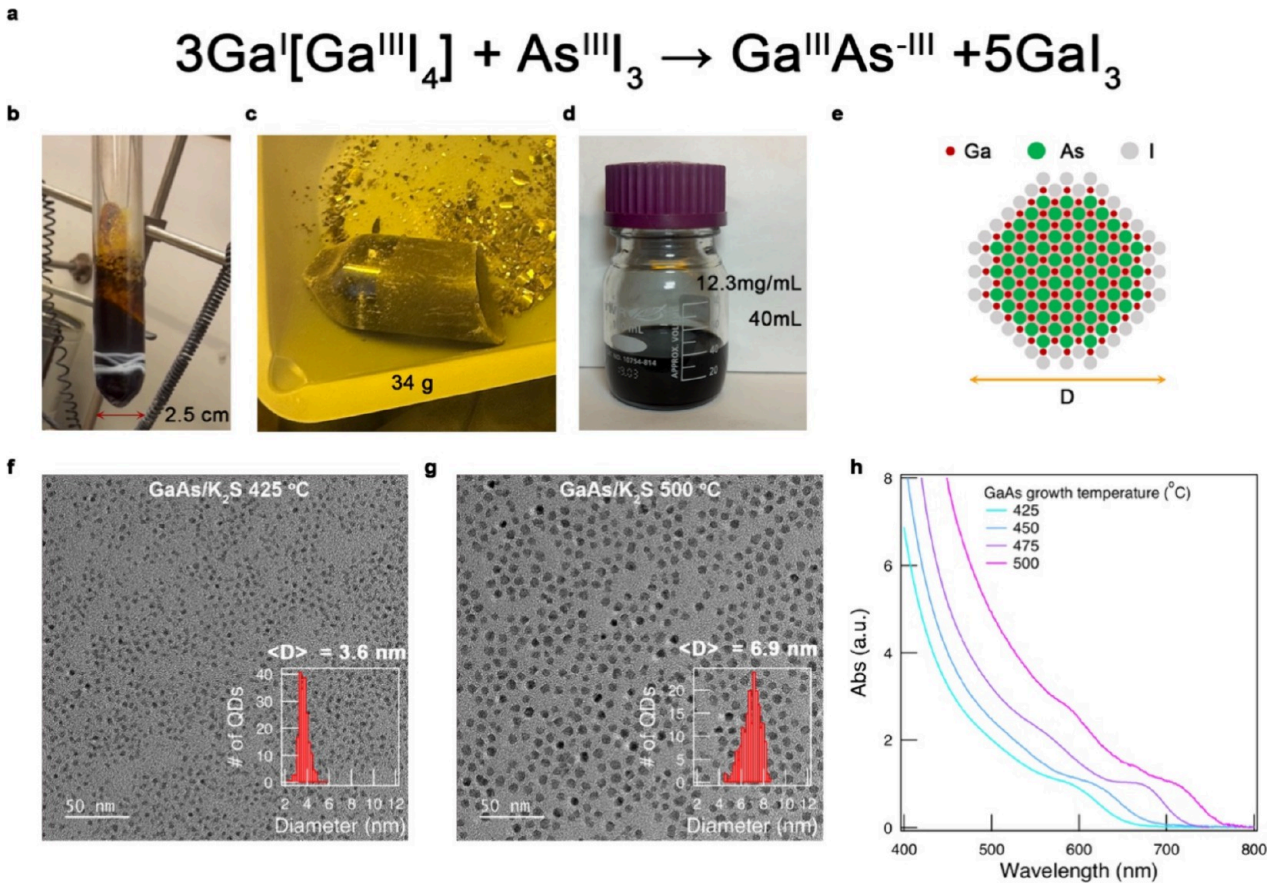

Figure 1. Large-scale synthesis of GaAs QDs in molten salt, followed by K_2S treatment. (a), (b) Large-scale synthesis showing the 1-in. outer diameter quartz ampule connected to Schlenk line, (c) crude product (34 g) after extraction from ampule, and (d) purified colloidal dispersion in toluene (40 mL, 12.3 mg/mL). (e) Schematic illustration of GaAs synthesized from molten salt. (f, g) TEM images of size-selected GaAs/K_2S cores synthesized at 425 °C (f) and 500 °C (g). Insets show size distributions (mean diameters 3.6 and 6.9 nm, respectively). Scale bars are 50 nm. (h) Absorption spectra of GaAs/K_2S cores at different synthesis temperatures, showing size-dependent excitonic features.

fine structure compared with other II−VI and III−V colloidal QDs.

In this work, we report the synthesis of GaAs QDs on a large (~500 mg) scale, their size-selective precipitation to obtain uniform size distributions, and molten-salt treatment of the GaAs surfaces with K_2S, followed by the growth of ZnSe/ZnS shells. Structural characterization confirmed conformal shell formation, while low-temperature optical measurements revealed the exciton fine structure in GaAs/ZnS QDs. Together, these results add GaAs to the list of established colloidal QD systems and provide new insights into the synthesis and properties of colloidal III−V QDs synthesized in molten salts, advancing their potential for next-generation optoelectronic and quantum technologies.

RESULTS AND DISCUSSION

Synthesis of the GaAs Core

GaAs QDs were synthesized following a previously reported procedure with minor modifications. Briefly, reduced gallium iodide (Ga_2I_4) was reacted with AsI_3 in molten alkali iodide salts above the critical temperature (400 °C) at which crystalline GaAs forms. We conducted reactions at 425, 450, 475, and 500 °C to achieve emissive colloidal GaAs QDs. Detailed methods can be found in Supplementary Note 1. We scaled a GaAs QD synthesis[29] to 33 g total reactant mass to obtain sufficient material for systematic optimization. Alkali iodide salts (NaI, KI, CsI) were dried under vacuum, and gallium iodide and reduced gallium iodide (GaI_3, Ga_2I_4) were synthesized from elemental precursors as described in Supporting Information (Supplementary Note 1). Reactions in Schlenk line-connected 1-inch-diameter ampules heated in a furnace for 1 h produced stable colloidal dispersions in the molten salt medium (Figure 1a−c and Supplementary Video 1). The resulting QDs were purified by dissolving the salt matrix in polar solvents and transferring the QDs to nonpolar solvents via ligand addition, ultimately yielding nearly 500 mg of purified GaAs QDs capped with oleylamine and gallium iodide that form stable colloidal dispersions in nonpolar organic solvents (Figure 1d).

By changing the reaction temperature, we could control the diameter of the GaAs core (Figure 1e). Size-selective precipitation of surface-treated GaAs QDs narrowed the size distribution and improved shape uniformity across all synthesis temperatures (Figure 1f,g and Supporting Information, Figure 1). The size-selected samples exhibited well-resolved excitonic absorption features, with the first exciton peak tunable from approximately 600−720 nm depending on the synthesis temperature (Figure 1h). Analysis of individual size fractions revealed that both particle size and shape varied across the distribution, contributing to inhomogeneous broadening in as-synthesized samples (Supporting Information, Figure 2), which is likely improvable by adding additional refinements, such as

https://doi.org/10.1021/jacs.6c03474
J. Am. Chem. Soc. 2026, 148, 22804−22816

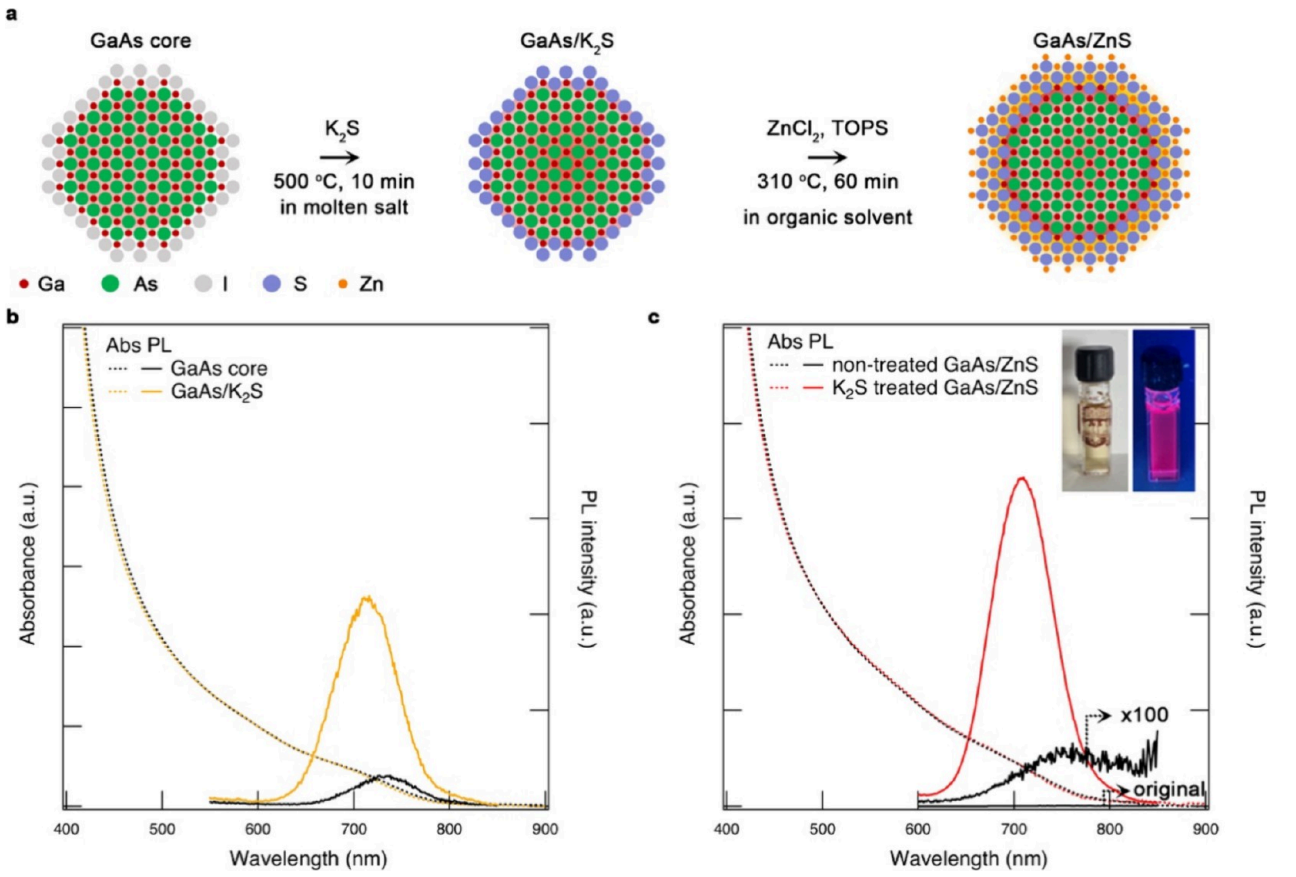

Figure 2. Synthesis and optical properties of K_2S-passivated GaAs/ZnS quantum dots. (a) Schematic of the synthesis: GaAs cores are treated with K_2S in molten salt, then passivated with ZnS via shell growth in the organic solvent. Absorption (dashed) and photoluminescence (solid) spectra of (b) GaAs QDs with (yellow) and without (black) K_2S treatment and (c) GaAs/ZnS QDs with (red) and without (black) K_2S treatment; for the untreated sample, having a GaAs concentration comparable to that of the treated sample, both the original PL spectrum and a magnified × 100 spectrum are shown. Inset: photographs under ambient (left) and UV (right) illumination.

improved mixing of the molten salt medium during QD synthesis.

Surface Treatment of GaAs QDs with K_2S

Initial attempts to grow zinc chalcogenide shells directly on as-synthesized GaAs cores in organic solvents failed to improve, and in fact degraded, the photoluminescence (PL), yielding essentially nonemissive materials. Drawing inspiration from sulfide passivation strategies developed for GaAs thin films,[30−32] we introduced a K_2S treatment step in molten salt prior to shell growth. In a typical treatment, 0.1 mmol of K_2S was added and ground into the molten-salt mixture containing GaAs QDs, followed by reheating at 500 °C for a defined duration. This surface modification proved essential: K_2S-treated GaAs cores supported uniform ZnS shell growth in organic media, with PL quantum efficiency improvements exceeding 2 orders of magnitude as compared to untreated cores (Figure 2a,c).

The K_2S surface treatment enhanced PL intensity by a factor of 3−5 while leaving the absorption spectrum unchanged, consistent with passivation of nonradiative surface trap states rather than modification of QD size or shape (Figure 2b). A slight blue shift of the emission maximum accompanied this intensity increase, which can be indicative of the passivation of shallow surface traps.

The surfaces of the as-synthesized GaAs cores, terminated by oleylamine and gallium iodide species, proved incompatible with conventional shell-growth protocols. ZnS shell growth using $ZnCl_2$ and trioctylphosphine sulfide (TOPS) at 310 °C, conditions that work well for InGaP and InGaAs QDs,[26,28] produced no PL enhancement and instead accelerated surface degradation (Figure 2c, black solid line). In contrast, K_2S treatment at 500 °C in molten salt created a sulfide-terminated surface that enabled conformal ZnS shell growth with dramatically improved optical properties (Figure 2c, red solid line). Photographs of the resulting GaAs/ZnS dispersions show bright red emission under UV illumination despite the emission maximum near 710 nm lying predominantly in the near-infrared (Figure 2c, inset).

To understand the surface chemistry underlying the optical improvements, we systematically characterized GaAs QDs treated with K_2S at temperatures ranging from 450 to 550 °C (Figure 3a). X-ray fluorescence (XRF) analysis revealed a clear temperature threshold for anion exchange. Below 500 °C, surfaces remained iodine-terminated with negligible sulfur incorporation, whereas at 500 °C and above, the sulfur content increased substantially while iodine content decreased (Figure 3b). This compositional transition coincided well with the onset of PL enhancement. The iodine to sulfur exchange was not exactly in the ratio of 2:1, presumably due to surface oxide present in as-synthesized GaAs QDs, which we discuss later.

Optical absorption spectra remained unchanged across all treatment temperatures (Figure 3d), confirming that K_2S exposure does not alter QD size or induce additional growth.

https://doi.org/10.1021/jacs.6c03474
J. Am. Chem. Soc. 2026, 148, 22804−22816

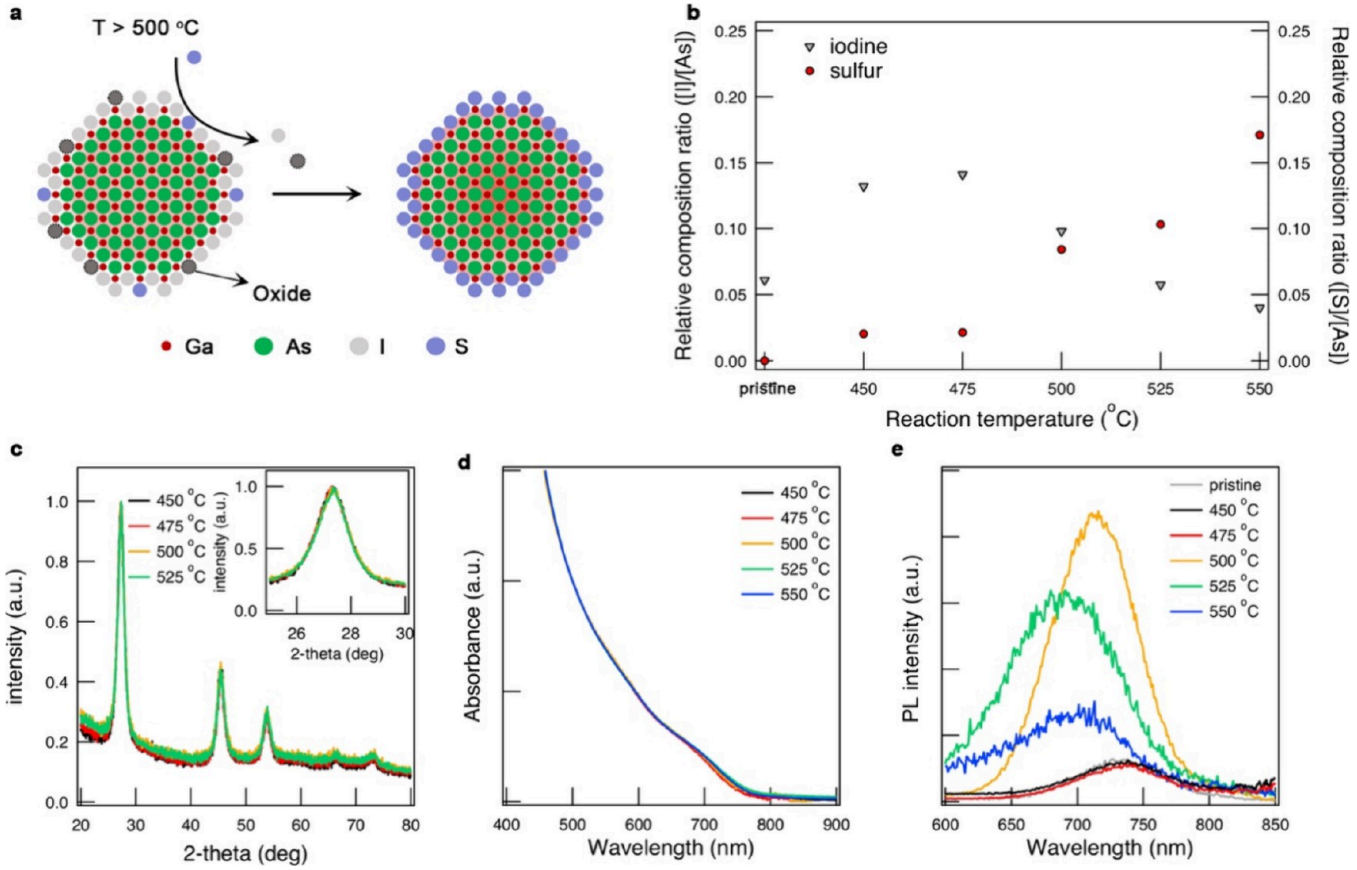

Figure 3. K_2S surface treatment removes oxide and passivates GaAs quantum dot surfaces. (a) Schematic of surface modification: iodine ligands and surface oxide are replaced by sulfide at temperatures above 500 °C. (b) Relative atomic ratios of iodine (I/As, gray triangles) and sulfur (S/As, red circles) versus treatment temperature, determined by XRF. (c) XRD patterns confirming retention of the zinc blende structure; inset shows the (111) reflection. (d) Absorption spectra after K_2S treatment at various temperatures, showing preservation of the optical gap. (e) Photoluminescence spectra showing maximal intensity for QDs treated with K_2S at 500 °C.

In contrast, PL behavior showed a strong temperature dependence (Figure 3e). Below the 500 °C threshold, emission intensity remained comparable to that of pristine GaAs QDs. At 500 °C, PL intensity increased markedly, consistent with effective surface trap passivation. Treatment at higher temperatures (525−550 °C) produced a slight blue-shift in emission but reduced intensity, suggesting an optimal passivation window near 500 °C. In addition to changes in the emission spectra, the ultraviolet photoemission spectroscopy (UPS) measurements showed that electron and hole energy levels of GaAs QDs shifted downward after the surface treatment, as surface iodine and oxygen were exchanged with sulfur (Supplementary Figure 3).

Structural characterization confirmed that sulfide treatment preserves the GaAs crystal structure without forming secondary phases. X-ray diffraction patterns (Figure 3c) showed zinc blende GaAs reflections, with no evidence of Ga_2S_3 or other impurity phases, and the (111) peak position and width remained constant across treatment conditions (Figure 3c, inset). Raman spectroscopy corroborated this finding; no peaks appeared near 233 cm^{-1}, where signatures from Ga_2S_3 would be expected (Supplementary Figure 4). The only spectral change observed was a shift of the longitudinal optical (LO) phonon mode toward the value tabulated for bulk GaAs (~292 cm^{-1}) accompanied by peak narrowing, indicative of the improved crystalline quality following sulfide passivation. Peaks from surface optical (SO) and transverse optical (TO) modes showed similar trends (Supplementary Figure 5).

In addition to surface passivation by sulfur, K_2S treatment also removes surface oxides from GaAs QDs, as evidenced by X-ray photoelectron spectroscopy (XPS). For comparison, we performed similar sulfide treatments, using both $(NH_4)_2S$ and K_2S, on bulk GaAs wafers, where oxide removal by sulfide passivation is well established.[30−32] The Ga 2p spectra (Figure 4a) showed characteristic changes upon sulfide treatment. Untreated GaAs wafers exhibited an asymmetric peak skewed toward higher binding energy, indicative of Ga−O bonding, which shifted to lower binding energy and sharpened after sulfide treatment. GaAs QDs displayed analogous behavior, with the Ga 2p peak shifting to lower binding energy after K_2S treatment in molten salt. Ga LMM Auger spectra revealed an oxide-related feature near 425 eV in untreated samples that disappeared after sulfide treatment for both wafers and QDs (Figure 4b). Ga 3d spectra (Figure 4c) exhibited subtle changes.

The As LMM, 3p, 3d spectra (Figure 4d−f) showed more subtle changes. Especially, As 3d spectra (Figure 4f) from untreated GaAs wafers exhibited a distinct high-binding-energy shoulder from 43−44 eV attributable to As−O species, which diminished upon sulfide treatment. For GaAs QDs, the As 3d peak shape changed less dramatically but showed narrowing on the high-binding-energy side after K_2S treatment. This asymmetry in oxide removal, more pronounced for gallium

https://doi.org/10.1021/jacs.6c03474
J. Am. Chem. Soc. 2026, 148, 22804−22816

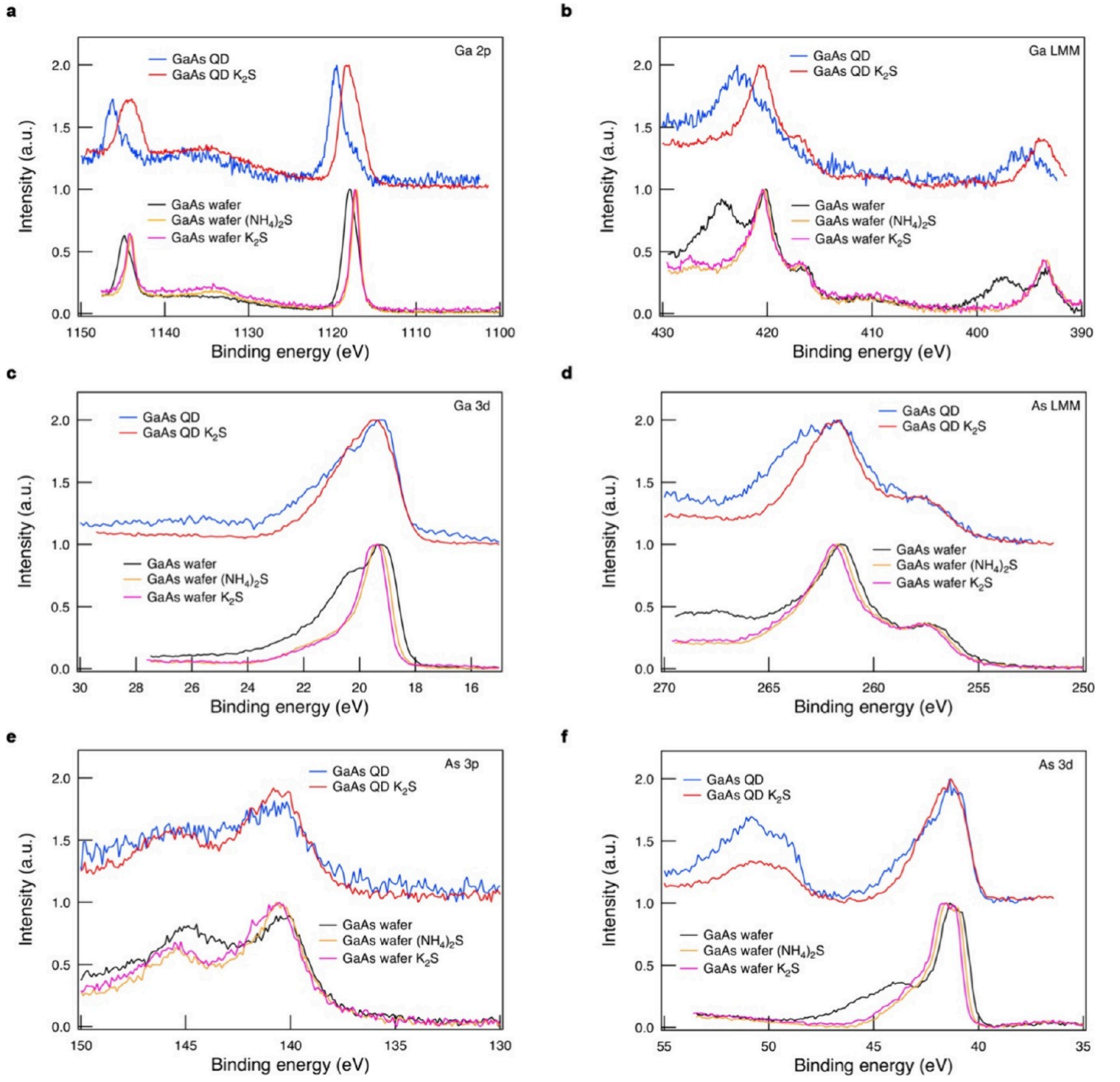

Figure 4. X-ray photoelectron spectroscopy of GaAs QDs and GaAs wafer references. High-resolution XPS spectra comparing GaAs QDs (blue) and GaAs QDs/K_2S (red) with GaAs single crystal (wafer) references: pristine (black), $(NH_4)_2S$-treated (orange), and K_2S-treated (magenta). Spectra are shown from (a) Ga 2p, (b) Ga LMM Auger, (c) Ga 3d, (d) As LMM Auger, (e) As 3p, and (f) As 3d core levels. The QD spectra show broader peaks compared to those from wafer references due to size-dependent effects and surface contributions.

than arsenic, likely reflects the gallium-rich surface termination typical of colloidal III−V nanocrystals. We attribute the initial surface oxidation to trace oxygen in the quartz reaction vessel or glovebox environment. Experiments using boron nitride or silicon nitride liners showed no significant differences in the final optical properties of core/shell QDs, suggesting that K_2S treatment effectively removes adventitious oxides regardless of their origin.

Influence of K_2S Treatment on Shell Growth of GaAs QDs

Having established optimal K_2S treatment conditions, we investigated how surface passivation influences the zinc chalcogenide shell growth. We deposited shells on both K_2S-treated and untreated GaAs cores by using identical reaction conditions to isolate the effect of surface chemistry. The structural and optical outcomes differed dramatically between the two cases (Figure 5a). High-angle annular dark-field scanning transmission electron microscopy (HAADF-STEM) combined with energy-dispersive X-ray spectroscopy (EDS) mapping revealed a pronounced difference in shell morphologies. On untreated GaAs cores, ZnSe was deposited nonuniformly, forming discontinuous islands with incomplete surface coverage (Figure 5b). In contrast, K_2S-treated cores supported conformal, continuous ZnSe shells with uniform elemental distribution (Figure 5c).

We attribute this difference to two factors: First, the strong Ga-amine surface bonds on untreated GaAs inhibit uniform Zn chalcogenide nucleation. Once nucleation occurs at isolated

https://doi.org/10.1021/jacs.6c03474
J. Am. Chem. Soc. 2026, 148, 22804−22816

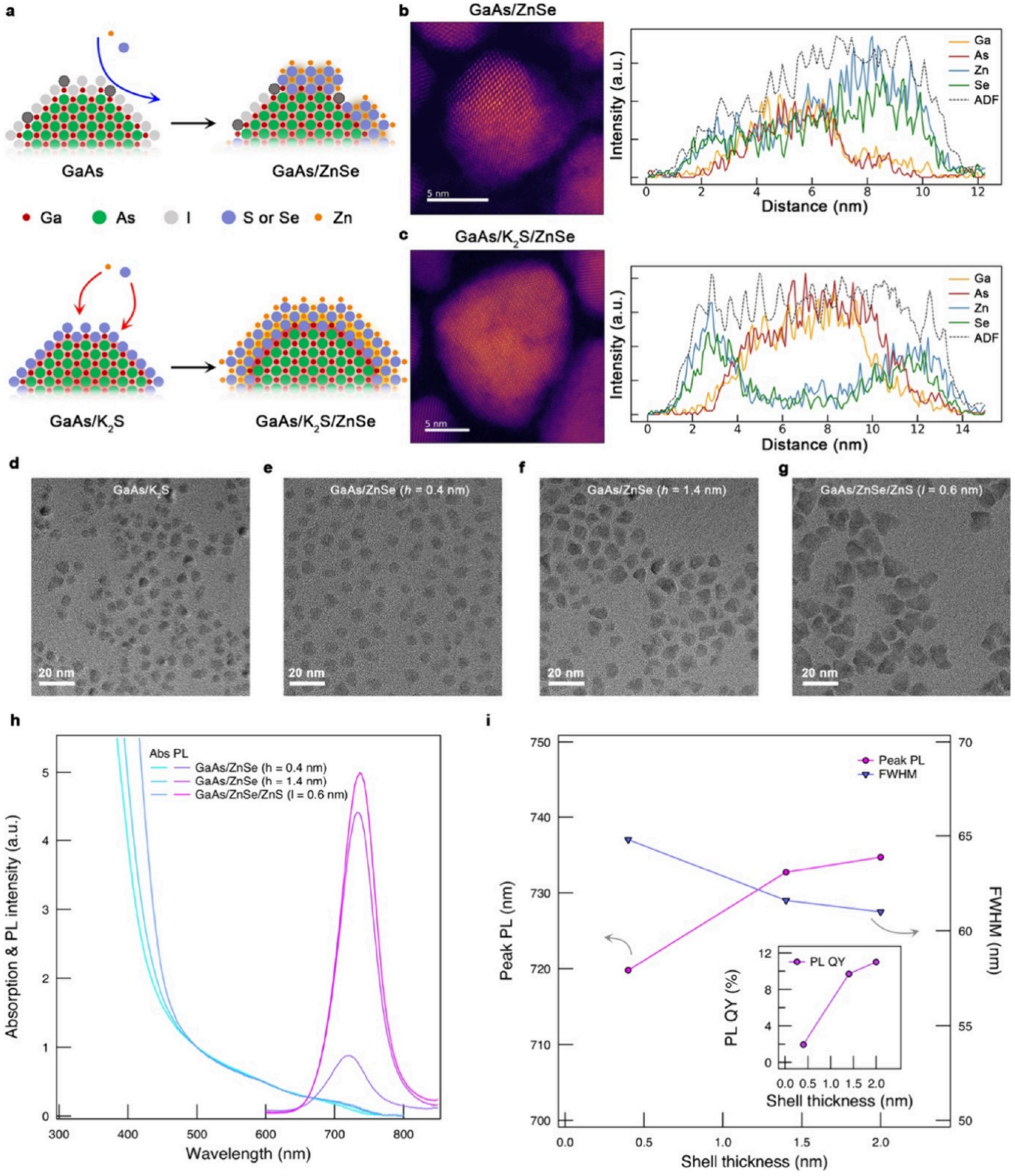

Figure 5. K_2S surface passivation enables uniform zinc chalcogenide shell growth on GaAs quantum dots. (a) Schematic comparing shell growth on untreated GaAs (top) versus K_2S-treated GaAs (bottom). Without K_2S treatment, heterogeneous growth produces nonuniform coverage; K_2S treatment provides a sulfide-terminated surface that promotes more uniform shell growth. (b) HAADF-STEM image and EDS line profiles of GaAs/ZnSe QDs grown without K_2S treatment. The elemental distributions of Ga, As, Zn, and Se show asymmetry, indicating nonuniform and discontinuous ZnSe shell growth around the GaAs core. The original HAADF-STEM image annotated with the exact EDS line-scan path is provided in Supplementary Figure S6. (c) HAADF-STEM image and EDS line profiles of GaAs/K_2S/ZnSe QDs. Following K_2S surface passivation, the Zn and Se signals form a well-defined, concentric shell surrounding the GaAs core, demonstrating uniform and conformal ZnSe shell growth. Scale bars, 5 nm. (d–g) TEM images showing the sequential shell growth stages: GaAs/K_2S core (d), GaAs/ZnSe with thin ZnSe shell (h = 0.4 nm) (e), GaAs/ZnSe with thick ZnSe shell (h = 1.4 nm) (f), and GaAs/ZnSe/ZnS (h = 1.4 nm, l = 0.5 nm) (g), where h and l denote the ZnSe and ZnS shell thicknesses, respectively. Scale bars, 20 nm. (h) Absorption (blue solid) and photoluminescence (pink solid) spectra during shell

https://doi.org/10.1021/jacs.6c03474
J. Am. Chem. Soc. 2026, 148, 22804–22816

Figure 5. continued

growth, with shell thicknesses indicated. (i) Peak emission wavelength (pink circles) and fwhm (blue triangles) versus total shell thickness; inset shows room temperature photoluminescence quantum yield reaching 10% for the final structure.

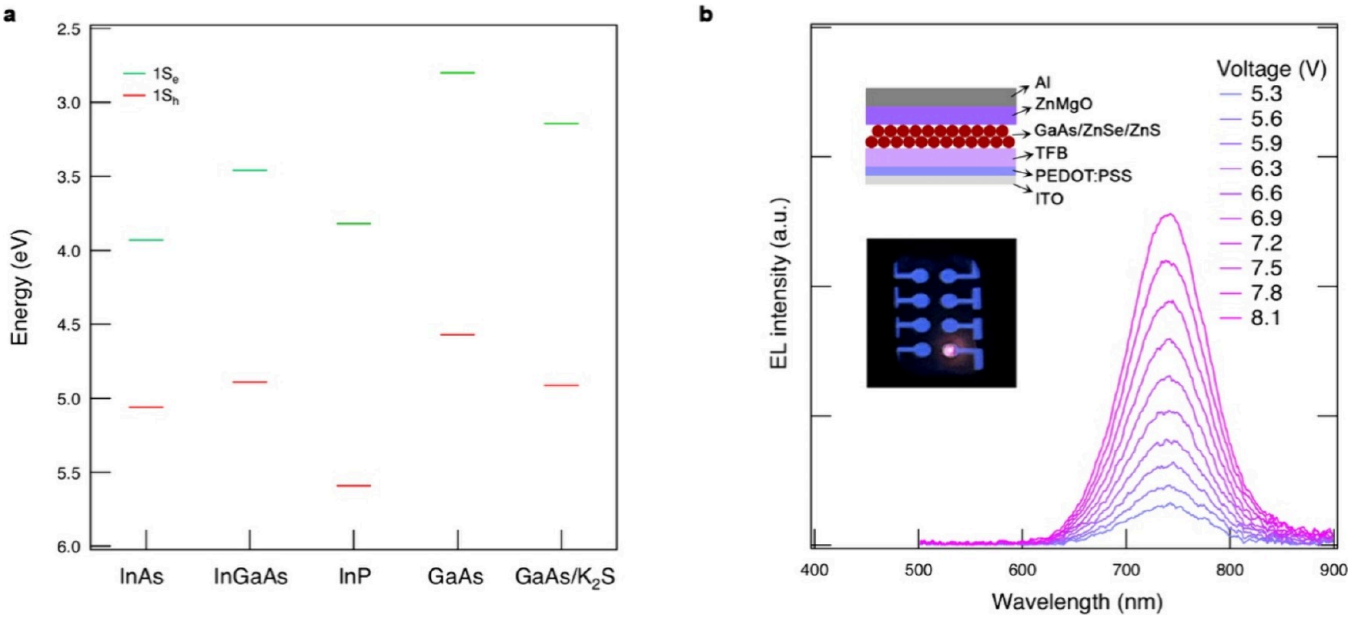

Figure 6. Energy levels of GaAs QDs and electroluminescence from GaAs QD-based light emitting diodes. (a) Energy level of III−V QDs including InAs, InGaAs, InP, and GaAs measured by UPS. For GaAs QDs, energy levels are shown before (GaAs) and after (GaAs/K_2S) surface treatment. (b) Electroluminescence spectra at varying voltages for a device with structure ITO/PEDOT:PSS/TFB/GaAs-ZnSe-ZnS/ZnMgO/Al. Inset: device schematic (top) and picture of operating device (bottom).

sites, subsequent growth occurs preferentially at those locations, leading to the formation of islands. Second, surface oxides, which K_2S treatment removes, create heterogeneous nucleation barriers that further promote nonuniform deposition, as in the case of InP QDs.[33] Structurally, island-like shells formed on untreated cores exhibit a higher density of stacking faults, whereas conformal shells grown on passivated cores show improved crystallinity with fewer defects (Figure 5b,c). Lower-magnification images confirmed these trends across entire QD populations (Supporting Information, Figure 7). Consistent with this interpretation, ZnS shell growth was strongly suppressed on untreated GaAs cores, resulting in nearly bare cores, whereas K_2S-treated cores exhibited uniform ZnS shell formation (Supporting Information, Figure 8).

The choice of the shell material profoundly influences the optical properties of GaAs-based core/shell QDs. ZnS shells induced a progressive blue shift in emission wavelength with increasing thickness, consistent with compressive strain arising from the 4% lattice mismatch between GaAs and ZnS. In contrast, ZnSe, which is nearly lattice-matched to GaAs, produced a red shift due to partial electron delocalization into the shell, enabled by the small conduction band offset (Supporting Information, Figure 9). The emission line widths evolved differently as well. Full-width at half-maximum (fwhm) increased during ZnS shell growth but decreased for ZnSe shells (Supporting Information, Figure 10). Time-resolved PL measurements revealed that ZnS shells progressively suppressed fast nonradiative decay components with increasing thickness, whereas QDs with ZnSe shells, despite improving emission intensity, retained significant fast decay channels (Supporting Information, Figure 9). This behavior reflects the different electron confinement provided by each material. Specifically, the larger conduction band offset of ZnS more effectively blocks electron trapping at the surface states.

These complementary attributes motivated us to develop a GaAs/ZnSe/ZnS heterostructure combining the advantages of both shell materials, as in the case of InP-based heterostructures.[10,34] The ZnSe inner shell provides a lattice-matched, low-strain interface to the GaAs core, while the ZnS outer shell supplies strong electron confinement and environmental protection. TEM imaging confirmed uniform, sequential shell deposition at each stage (Figure 5d−g). The resulting GaAs/ZnSe/ZnS QDs exhibited narrow emission line widths comparable to those from GaAs/ZnSe QDs (fwhm ∼60 nm, 140 meV) together with the bright emission characteristic of GaAs/ZnS QDs (Figure 5h,i, Supporting Information, Figure 11, and Table S3). Optimizing the synthesis of cores with the graded shell architecture yielded QDs with PL quantum yields reaching 10%, a substantial improvement for GaAs QDs and a key step toward their practical optoelectronic applications.

GaAs QDs exhibit significantly higher energy states compared to other III−V QDs, resulting in a larger energy offset relative to environmental levels (Figure 6a). The UPS spectra and the procedure used to extract valence band maxima and band gap of QDs are provided in Supporting Information, Figure 3. This elevated $1S_h$ position suppresses $1S_h$ hole trapping and favors $1S_e$ electron trapping as the dominant charge localization pathway, in contrast to InP QDs, where hole trapping is prevalent. The unique energy-level alignment of GaAs QDs distinguishes them from other III−V QDs and has important implications for charge balance and recombina-

https://doi.org/10.1021/jacs.6c03474
J. Am. Chem. Soc. 2026, 148, 22804−22816

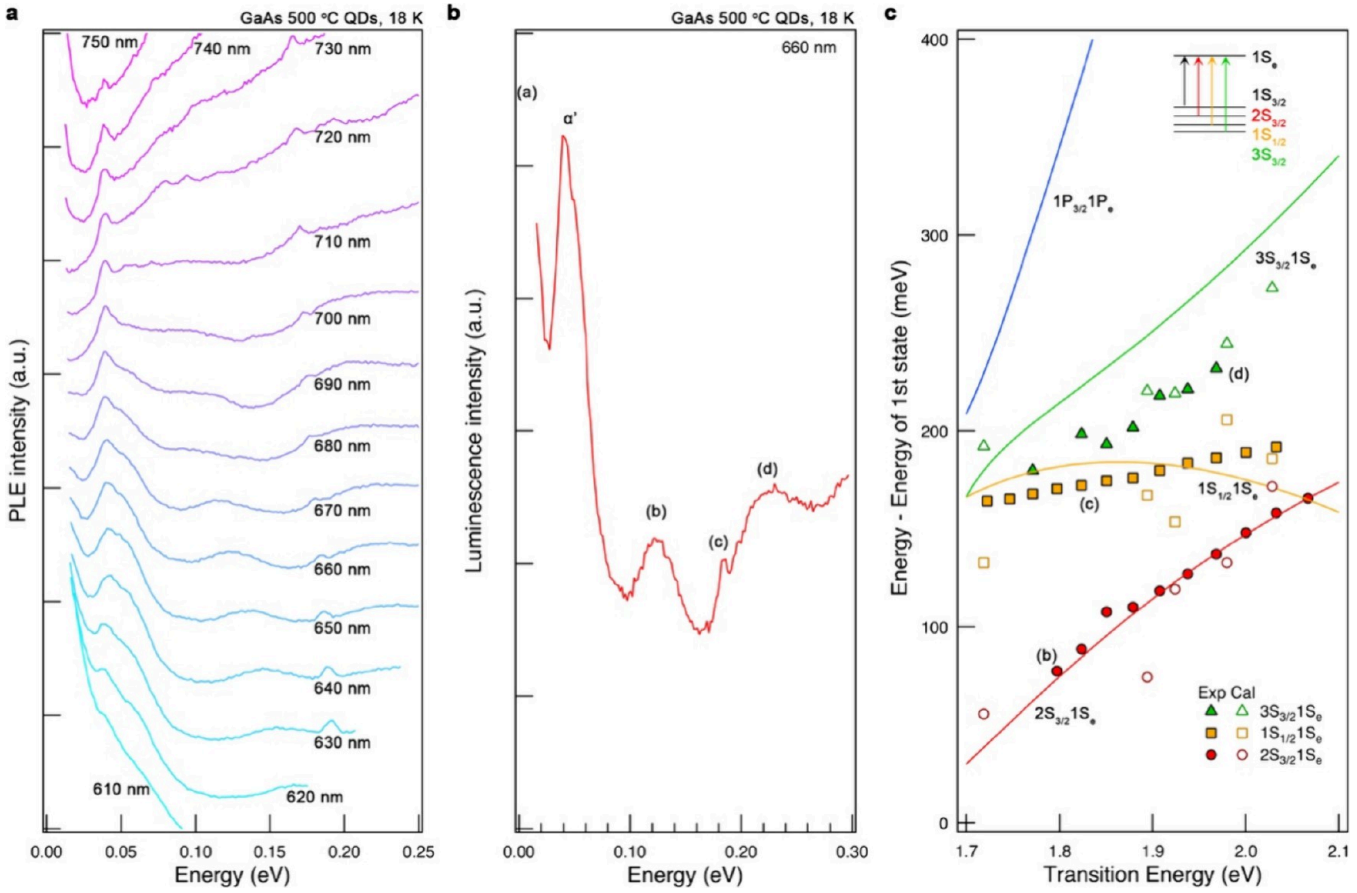

Figure 7. Optical transitions in GaAs/ZnS quantum dots. (a) Photoluminescence excitation (PLE) spectra recorded at 18 K for GaAs/ZnS QDs (GaAs cores synthesized at 500 °C) detected at emission wavelengths from 610 to 750 nm, revealing discrete excited-state transitions. (b) Representative PLE spectrum detected at 660 nm; peaks (b–d) correspond to transitions involving higher-energy hole states. (c) Transition energies extracted from PLE (solid symbols) versus emission energy curves with theoretical calculations based on an effective mass model (solid curves), and the DeepPseudopot model (hollow symbols). Inset: schematic of electron ($1S_e$) and hole ($1S_{3/2}$, $2S_{3/2}$, $1S_{1/2}$, $3S_{3/2}$) energy levels.

tion dynamics in devices. We adopted a QD-based light-emitting diode structure that was optimized for InP QDs to test device performance. Devices with the structure ITO/PEDOT:PSS/TFB/GaAs-ZnSe-ZnS/ZnMgO/Al exhibited electroluminescence across a range of operating voltages (Figure 6b), demonstrating that molten salt-derived GaAs QDs can be integrated into functional optoelectronic devices but need further optimization. Current–voltage–luminance (J–V–L) characteristics of representative devices are provided in Supporting Information, Figure 12.

Excitonic Transitions and Exciton Fine Structure of GaAs QDs

The improved optical quality of GaAs QDs enabled a detailed investigation of their excitonic transitions and exciton fine structure. These fundamental properties of QDs have been extensively characterized for II–VI (mostly CdSe)[35,36] and III–V (InP and InAs) semiconductors,[37−39] but have not been explored for Ga-based colloidal III–V QDs. We employed fluorescence line-narrowing (FLN) and photoluminescence excitation (PLE) spectroscopy at cryogenic temperatures (13–20 K) to resolve discrete electronic transitions. For these studies, we chose GaAs/ZnS QDs, which exhibited a QY of about 3%, because of large energy offsets at the core–shell interface, which efficiently confine the electron and hole wave functions in the GaAs core and minimize state mixing between the core and the shell. Upon cooling from room temperature to 20 K, the PL intensity increased by approximately an order of magnitude (Supplementary Figure 13), suggesting that the quantum yield of these GaAs/ZnS QDs approached at least 30% at low temperatures.

PLE and FLN spectra have been measured from multiple GaAs/ZnS samples with cores synthesized at 425, 450, 475, and 500 °C (Supplementary Figure 14). PLE spectra recorded at different emission wavelengths spanning the 610–750 nm range revealed multiple discrete absorption features above the band edge (Figure 7a). We observed several optical transitions related to higher hole states from PLE peaks, labeled (b–d) in a representative spectrum detected at 660 nm emission (Figure 7b), which are identified as the transitions from different hole states ($2S_{3/2}$, $1S_{1/2}$, and $3S_{3/2}$) to the $1S_e$ state. By changing the detected emission wavelength, we observed the size-dependent properties of each transition (Figure 7c). The energy separations between the transitions vary systematically with GaAs QD size, as expected for quantum-confined systems. Fitting the size-dependent transition energies to an effective mass model with finite barrier height (Figure 7c and Supplementary Note 3) allowed assignment of the observed PLE peaks to transitions involving the $1S_{3/2}$, $2S_{3/2}$, $1S_{1/2}$, and $3S_{3/2}$ hole levels. The exciton transition energy separations and their size dependence were also calculated using DeepPseudopot, a machine-learned semiempirical pseudopotential framework (Supplementary Note 3).[40] The effective mass

https://doi.org/10.1021/jacs.6c03474
J. Am. Chem. Soc. 2026, 148, 22804–22816

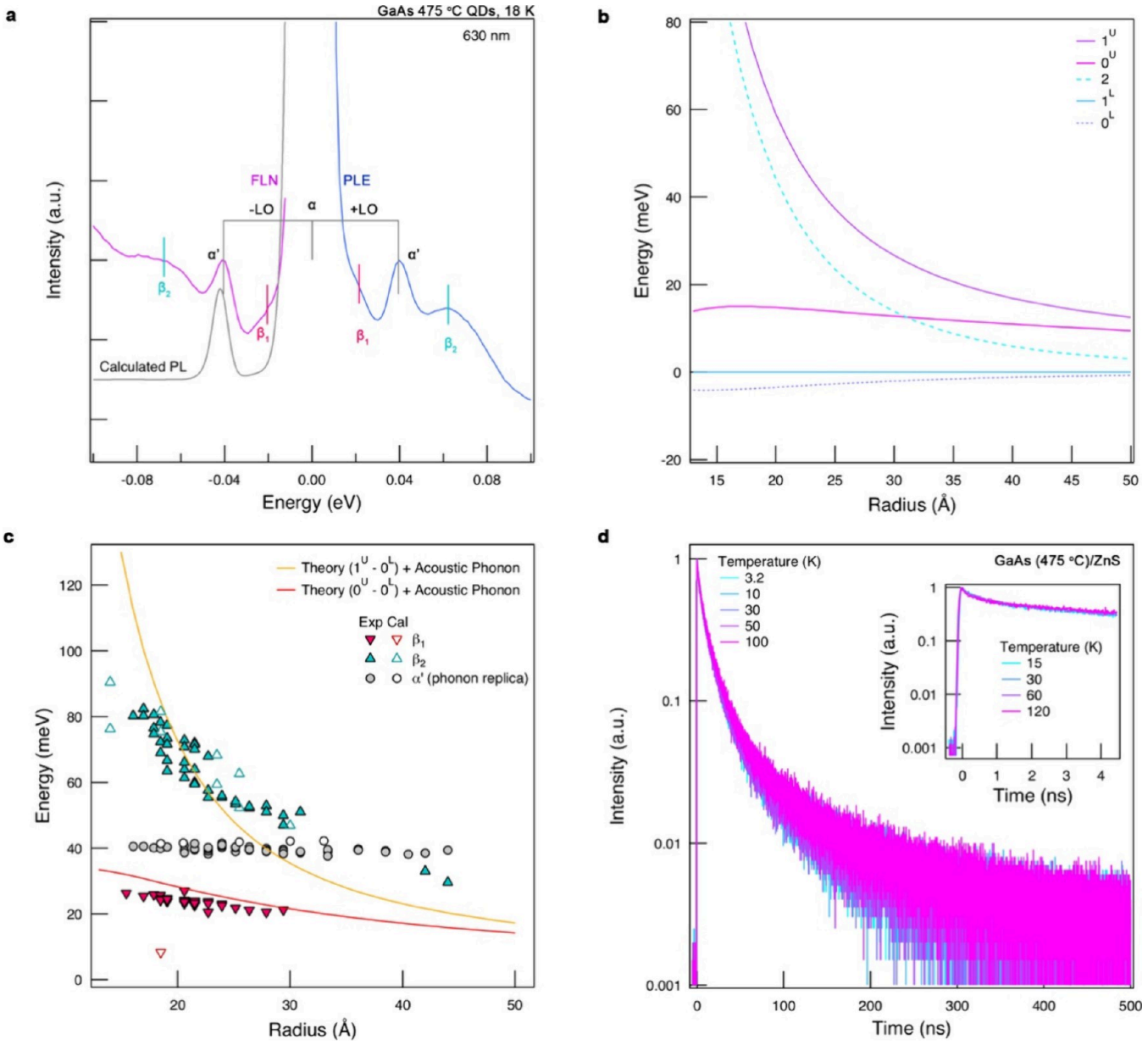

Figure 8. Exciton fine structure and recombination dynamics in GaAs/ZnS quantum dots. (a) Representative comparison of fluorescence line-narrowing (FLN, pink), PLE (cyan), and the calculated PL (gray) spectra from GaAs/ZnS QDs emitting at 630 nm. The zero-phonon line (α) and its LO phonon replicas (α') are indicated, along with fine-structure features β_1 and β_2. (b) Calculated exciton fine-structure energies as a function of QD radius, showing the evolution of bright ($\pm1^u$, 0^u, $\pm1^L$) and dark (0^L, ±2) states. (c) Bright-state splitting energies: experimental values (triangles) compared with theoretical predictions for $\pm1^u-0^L$ (yellow) and 0^u-0^L (red) transitions using the effective mass model,[36] and DeepPseudopot model exciton fine structure calculations (hollow colored symbols). Gray circles indicate LO phonon replica positions and gray hollow circles indicate the LO phonon sideband locations calculated using the DeepPseudopot method. (d) Temperature-dependent photoluminescence decay spectra from 3.2 to 100 K, showing negligible variation; inset shows PL decay as measured by a streak camera.

model and pseudopotential calculations both yield results consistent with the level ordering expected for GaAs QDs. We noticed a slightly better agreement for the higher-energy states from the pseudopotential calculation, which may reflect an overestimation of the transition energies by the effective mass method arising from the infinite potential barrier approximation for the hole. For comparison, we measured K_2S-treated GaAs cores without shells; although the weaker signal precluded complete analysis, the same general spectral features were observed (Supplementary Figure 15). Somewhat surprisingly, within the measured window of energies up until 0.3 eV above the $1S_{3/2}-1S_e$ transition, we have not observed any transitions related to electron states from different momentum valleys, such as the L-valley, which was believed to be closely aligned under quantum confinement and could even become the lowest transition state when QD diameter is under 3.2 nm.[41−44]

Representative comparisons between FLN and PLE spectra for quantum dots emitting at 630 nm reveal multiple peaks corresponding to (i) the LO phonon replicas of the zero phonon line (ZPL, α) labeled as α' and (ii) distinctive exciton fine structure features β_1 and β_2 (Figure 8a). Theoretical modeling of the exciton fine structure as a function of quantum dot radius based on the effective mass model shows the

https://doi.org/10.1021/jacs.6c03474
J. Am. Chem. Soc. 2026, 148, 22804−22816

evolution of exciton fine structure splitting under quantum confinement (Figure 8b). Detailed calculation methods are explained in Supporting Information (Supplementary Note 3). To understand the phonon replicas, we also modeled phonon frequencies, exciton−phonon coupling (EXPC) strengths, and their size dependence using DeepPseudopot,[40] combined with a Tersoff-type force field[45] (Supplementary Figures S16, S17, and Supplementary Note 3). The acoustic phonon modes with the strongest coupling to band-edge excitons have frequencies that scale inversely with QD size, whereas the LO phonon frequencies show minimal size dependence, consistent with their bulk-like Ga−As relative optical vibration. Phonon-resolved single-QD linear emission spectra were computed from the EXPC within the linear response theory. At low temperatures, the calculated spectra show an LO phonon replica at ∼42 meV from the ZPL, which is consistent with the FLN and PLE measurements. A secondary lower acoustic phonon shoulder at ∼7−13 meV arises from modes with collective nuclear vibrations extending across the entire nanocrystal, such as twisting or breathing-like distortions, but it is not resolved in FLN or PLE due to its small energy spacing from the excitation source. With increasing QD size, the EXPC strength weakens, the phonon sideband intensities decrease, and the spectrum progressively simplifies.

Experimentally extracted bright-state-to-bright-state splittings, attributed to exchange interactions between electron and hole states, demonstrate relatively good agreement with theoretical predictions and show a clear size dependence with both effective mass and pseudopotential theoretical predictions (Figure 8c). The small deviation of β_2 at larger sizes of QD is expected to be due to the interactions between bright states and phonon-coupled modes, which have been observed in CuCl nanoparticles.[46]

Surprisingly, temperature-dependent PL decay measurements reveal that exciton recombination dynamics remain largely unchanged from 3.2 to 100 K (Figure 8d). This behavior has been observed in some cases of epitaxial III−V QDs.[47−49] To confirm the existence or absence of potential fast decay modes that were not detected by TCSPC measurements, we have measured PL spectra using a streak camera at low temperature, which show no distinctive fast decay at the picosecond time scale (Figure 8d, inset and Supplementary Figure 18). Several potential explanations for this absence could exist. First, very closely separated dark and bright states could lead to mixed emission even at 4 K. Although our EMA calculation expects a separation of 1−2 meV between dark (0^L) and bright states ($\pm1^L$), the actual dark−bright splitting could be significantly smaller. Second, carrier trapping may suppress the population or radiative contribution of the dark exciton, rendering its emission negligible. We modeled decay rates based on these bright-dark state splittings, including trap states, and this model described our observed exciton decay dynamics (Supplementary Figure 19 and Note 3.3) reasonably well. As this nonradiative rate significantly reduces the quantum yield of dark exciton decay modes, we could not observe decay from dark excitons. Furthermore, we performed low-temperature magneto-optic measurements on GaAs/ZnS particles embedded in a polymer matrix (Supplementary Figures 20 and 21). These measurements showed only minor changes in excitonic decay rates, consistent with the weak temperature dependence observed in these samples. Collectively, these results help the understanding of the electronic structure and photophysics of colloidal GaAs QDs in the strong confinement regime, which have not been accessed previously. This understanding should be further advanced and refined in future in-depth studies.

SUMMARY

In this work, we demonstrated emissive colloidal GaAs quantum dots (QDs) through colloidal synthesis in a molten inorganic salt, surface passivation, and growth of an epitaxial zinc chalcogenide shell. Using K_2S in a molten salt for GaAs QD surface treatment, we effectively removed surface oxides and enabled the uniform growth of Zn-based shells on the GaAs QDs. Structural characterization confirmed conformal shell formation, while low-temperature photoluminescence measurements revealed well-resolved excitonic fine structure of this technologically important but previously inaccessible QD material. The combination of size fractionation, surface treatments, and shell growth significantly improved both emission line width and photoluminescence efficiency. Spectroscopic studies of GaAs QDs have provided important clues on their electronic structure through excitonic transition energies and exciton fine structure, further corroborated by theoretical modeling. An unusual feature of GaAs QDs is the temperature-independent luminescence decay time, which may originate from the small splitting between the lowest dark and bright excitonic states.

These results provide new insights into the surface chemistry and excitonic behavior of colloidal III−V QDs, demonstrating that molten-salt colloidal synthesis and surface engineering are practical approaches to overcoming limitations in GaAs QDs. This work advances the fundamental understanding of colloidal III−V QDs and establishes a pathway for their integration into next-generation optoelectronic and quantum devices. Further optimizations of GaAs colloidal synthesis, followed by the improvements of III−V/II-VI heterovalent interfaces or the preparation of an all-III−V-based heterostructure, will likely lead to even higher-quality colloidal GaAs and III−V semiconductors.

ASSOCIATED CONTENT

Supporting Information

The Supporting Information is available free of charge at https://pubs.acs.org/doi/10.1021/jacs.6c03474.

Synthetic methods including syntheses of GaI_3, Ga_2I_4, alkali halide salts, and GaAs quantum dots, K_2S surface treatment, size-selective precipitation, and Zn chalcogenide shell growth; characterization methods (UV−vis−NIR absorption, room-temperature and cryogenic photoluminescence, time-correlated single photon counting, streak camera measurements, LED J−V−L characterization, Raman spectroscopy, PXRD, XPS, XRF, SAXS, and TEM); theoretical calculation methods with GaAs material parameters (Tables S1 and S2); TEM images of size-tunable GaAs/K_2S QDs synthesized at 425−500 °C (Figure S1); TEM images and absorption spectra of size-selective precipitation fractions (Figure S2); UPS derived energy-level alignment of GaAs, GaAs/K_2S, InP, InGaAs, and InAs QDs (Figure S3); Raman spectra and TO/SO/LO phonon-mode deconvolution as a function of sulfide treatment temperature (Figures S4 and S5); STEM-HAADF images and STEM-EDS elemental maps of GaAs/ZnSe and GaAs/ZnS core/shell QDs with and without K_2S

https://doi.org/10.1021/jacs.6c03474
J. Am. Chem. Soc. 2026, 148, 22804−22816

surface treatment (Figures S6–S8); shell thickness-dependent absorption, PL spectra, and PL decay curves of GaAs/ZnS and GaAs/ZnSe QDs (Figures S9 and S10); multishell GaAs/ZnSe/ZnS heterostructure optical properties (Figure S11); electroluminescence device characteristics (Figure S12); summary of optical properties of GaAs-based core/shell nanocrystals (Table S3); temperature-dependent PL of GaAs/ZnS QDs from 20 to 300 K (Figure S13); PLE and FLN spectra of GaAs/ZnS QDs (Figure S14); exciton fine-structure analysis of GaAs/K_2S QDs (Figures S15); theoretical modeling of exciton–phonon coupling spectral densities and phonon-resolved single-QD PL spectra (Figures S16 and S17); ultrafast streak-camera PL dynamics (Figure S18); exciton decay-rate modeling using a bright/dark exciton model with nonradiative decay (Figure S19); SAXS intensity profiles of GaAs/ZnS QDs dispersed in PMMA and PBMA-*co*-PiBMA matrices (Figure S20); and magnetic-field-dependent (0 and 6 T) PL decay (Figure S21) (PDF)

AUTHOR INFORMATION

Corresponding Author

Dmitri V. Talapin – *Department of Chemistry, James Franck Institute, and Pritzker School of Molecular Engineering, University of Chicago, Chicago, Illinois 60637, United States; Center for Nanoscale Materials, Argonne National Laboratory, Argonne, Illinois 60439, United States;* orcid.org/0000-0002-6414-8587; Email: dvtalapin@uchicago.edu

Authors

Jun Hyuk Chang – *Department of Chemistry, James Franck Institute, and Pritzker School of Molecular Engineering, University of Chicago, Chicago, Illinois 60637, United States;* orcid.org/0000-0003-1640-0343

Danial Zangeneh – *Department of Physics, University of Illinois Chicago, Chicago, Illinois 60607, United States;* orcid.org/0009-0009-0650-5230

Heng-Chi Chu – *Department of Chemistry, James Franck Institute, and Pritzker School of Molecular Engineering, University of Chicago, Chicago, Illinois 60637, United States*

Justin C. Ondry – *Department of Chemistry, James Franck Institute, and Pritzker School of Molecular Engineering, University of Chicago, Chicago, Illinois 60637, United States;* orcid.org/0000-0001-9113-3420

Kailai Lin – *Department of Chemistry, University of California, Berkeley, California 94720, United States; Materials Sciences Division, Lawrence Berkeley National Laboratory, Berkeley, California 94720, United States;* orcid.org/0000-0001-8509-5560

Yuan Liu – *Department of Chemistry, James Franck Institute, and Pritzker School of Molecular Engineering, University of Chicago, Chicago, Illinois 60637, United States*

Zirui Zhou – *Department of Chemistry, James Franck Institute, and Pritzker School of Molecular Engineering, University of Chicago, Chicago, Illinois 60637, United States;* orcid.org/0000-0001-6740-2432

Ahhyun Jeong – *Department of Chemistry, James Franck Institute, and Pritzker School of Molecular Engineering, University of Chicago, Chicago, Illinois 60637, United States;* orcid.org/0000-0002-5362-0700

James Cassidy – *Department of Chemistry, James Franck Institute, and Pritzker School of Molecular Engineering, University of Chicago, Chicago, Illinois 60637, United States;* orcid.org/0009-0009-6719-4245

Sungsu Kang – *Department of Chemistry, James Franck Institute, and Pritzker School of Molecular Engineering, University of Chicago, Chicago, Illinois 60637, United States;* orcid.org/0000-0001-8220-0345

Scott A. Crooker – *National High Magnetic Field Laboratory, Los Alamos National Laboratory, Los Alamos, New Mexico 87545, United States;* orcid.org/0000-0001-7553-4718

Alexander S. Filatov – *Department of Chemistry, James Franck Institute, and Pritzker School of Molecular Engineering, University of Chicago, Chicago, Illinois 60637, United States;* orcid.org/0000-0002-8378-1994

A. Paul Alivisatos – *Department of Chemistry, James Franck Institute, and Pritzker School of Molecular Engineering, University of Chicago, Chicago, Illinois 60637, United States*

Eran Rabani – *Department of Chemistry, University of California, Berkeley, California 94720, United States; Materials Sciences Division, Lawrence Berkeley National Laboratory, Berkeley, California 94720, United States; Fritz Haber Center for Molecular Dynamics, Institutes of Chemistry and Applied Physics, The Hebrew University of Jerusalem, Jerusalem 9190401, Israel;* orcid.org/0000-0003-2031-3525

Robert F. Klie – *Department of Physics, University of Illinois Chicago, Chicago, Illinois 60607, United States;* orcid.org/0000-0003-4773-6667

Richard D. Schaller – *Center for Nanoscale Materials, Argonne National Laboratory, Argonne, Illinois 60439, United States; Department of Chemistry, Northwestern University, Evanston, Illinois 60208, United States;* orcid.org/0000-0001-9696-8830

Alexander L. Efros – *U.S. Naval Research Laboratory, Washington, DC 20375, United States;* orcid.org/0000-0003-1938-553X

Complete contact information is available at: https://pubs.acs.org/10.1021/jacs.6c03474

Author Contributions

The manuscript was written through contributions of all authors. All authors have given approval to the final version of the manuscript.

Notes

The authors declare no competing financial interest.

ACKNOWLEDGMENTS

We thank Dr. A. Nelson for reading and editing the manuscript. We also thank Dr. J. Jureller for help with Raman measurements. The work on the synthesis of novel III–V quantum dots was supported by the National Science Foundation under Award No. CHE-2404291 and the Samsung QD Cluster Collaboration. Spectroscopic and computational studies of novel III–V quantum dots were supported by the National Science Foundation Science and Technology Center (STC) for Integration of Modern Optoelectronic Materials on Demand (IMOD) under Award No. DMR-2019444. J.C. acknowledges support from the National Research Foundation of Korea (NRF) grant funded by the Korea government (MSIT) (No. RS-2024-00359602). A.J. is partially supported by the Kwanjeong Educational Foundation. D.Z. and R.F.K.

acknowledge support from the National Science Foundation (NSF-CBET 2312359) and by the Army Research Office under Grant Number W911NF-23-1-0225. E.R. thanks the Israel Science Foundation for support (No. 4085/25) and acknowledges support from the National Science Foundation Division of Chemistry, under the Chemical Theory, Models and Computational Methods (CTMC) program, grant number CHE-2449564. Al. L.E. acknowledges support from the Office of Naval Research. The views and conclusions contained in this document are those of the authors and should not be interpreted as representing the official policies, either expressed or implied, of the Army Research Office or the U.S. Government. The U.S. Government is authorized to reproduce and distribute reprints for Government purposes, notwithstanding any copyright notation herein. This work made use of the shared facilities at the University of Chicago Materials Research Science and Engineering Center, supported by the National Science Foundation under award number DMR-2011854. Work performed at the Center for Nanoscale Materials, a U.S. Department of Energy Office of Science User Facility, was supported by the U.S. DOE, Office of Basic Energy Sciences, under Contract No. DE-AC02-06CH11357. The work performed at the National High Magnetic Field Laboratory is supported by National Science Foundation DMR-2128556, the US DOE, and the State of Florida.

REFERENCES

(1) Brus, L. Electronic Wave Functions in Semiconductor Clusters: Experiment and Theory. *J. Phys. Chem.* **1986**, *90* (12), 2555−2560.
(2) Colvin, V. L.; Schlamp, M. C.; Alivisatos, A. P. Light-Emitting Diodes Made from Cadmium Selenide Nanocrystals and a Semiconducting Polymer. *Nature* **1994**, *370* (6488), 354−357.
(3) Klimov, V. I.; Mikhailovsky, A. A.; Xu, S.; Malko, A.; Hollingsworth, J. A.; Leatherdale, C. A.; Eisler, H.-J.; Bawendi, M. G. Optical Gain and Stimulated Emission in Nanocrystal Quantum Dots. *Science* **2000**, *290* (5490), 314−317.
(4) Coropceanu, I.; Bawendi, M. G. Core/Shell Quantum Dot Based Luminescent Solar Concentrators with Reduced Reabsorption and Enhanced Efficiency. *Nano Lett.* **2014**, *14* (7), 4097−4101.
(5) Konstantatos, G.; Howard, I.; Fischer, A.; Hoogland, S.; Clifford, J.; Klem, E.; Levina, L.; Sargent, E. H. Ultrasensitive Solution-Cast Quantum Dot Photodetectors. *Nature* **2006**, *442* (7099), 180−183.
(6) Nozik, A. J. Quantum Dot Solar Cells. *Physica E: Low-dimensional Systems and Nanostructures* **2002**, *14* (1−2), 115−120.
(7) Murray, C. B.; Norris, D. J.; Bawendi, M. G. Synthesis and Characterization of Nearly Monodisperse CdE (E = Sulfur, Selenium, Tellurium) Semiconductor Nanocrystallites. *J. Am. Chem. Soc.* **1993**, *115* (19), 8706−8715.
(8) Hines, M. A.; Guyot-Sionnest, P. Synthesis and Characterization of Strongly Luminescing ZnS-Capped CdSe Nanocrystals. *J. Phys. Chem.* **1996**, *100* (2), 468−471.
(9) Micic, O. I.; Curtis, C. J.; Jones, K. M.; Sprague, J. R.; Nozik, A. J. Synthesis and Characterization of InP Quantum Dots. *J. Phys. Chem.* **1994**, *98* (19), 4966−4969.
(10) Won, Y.-H.; Cho, O.; Kim, T.; Chung, D.-Y.; Kim, T.; Chung, H.; Jang, H.; Lee, J.; Kim, D.; Jang, E. Highly Efficient and Stable InP/ZnSe/ZnS Quantum Dot Light-Emitting Diodes. *Nature* **2019**, *575* (7784), 634−638.
(11) Franke, D.; Harris, D. K.; Chen, O.; Bruns, O. T.; Carr, J. A.; Wilson, M. W. B.; Bawendi, M. G. Continuous Injection Synthesis of Indium Arsenide Quantum Dots Emissive in the Short-Wavelength Infrared. *Nat. Commun.* **2016**, *7* (1), 12749.
(12) Kim, T.; Park, S.; Jeong, S. Diffusion Dynamics Controlled Colloidal Synthesis of Highly Monodisperse InAs Nanocrystals. *Nat. Commun.* **2021**, *12* (1), 3013.
(13) Liu, W.; Chang, A. Y.; Schaller, R. D.; Talapin, D. V. Colloidal InSb Nanocrystals. *J. Am. Chem. Soc.* **2012**, *134* (50), 20258−20261.
(14) Holonyak, N.; Bevacqua, S. F. Coherent (Visible) Light Emission From $Ga(As_{1-x}P_x)$ Junctions. *Appl. Phys. Lett.* **1962**, *1* (4), 82−83.
(15) Schnitzer, I.; Yablonovitch, E.; Caneau, C.; Ersen, A.; Gmitter, T. J. Ultra-High Spontaneous Emission Quantum Efficiency, 99.7% Internally And 72% Externally, From AlGaAs/GaAs/AlGaAs Double Heterostructures. In *LEOS'92 Conference Proceedings*; IEEE: Boston, MA, 1992; pp 127−128.
(16) Hall, R. N.; Fenner, G. E.; Kingsley, J. D.; Soltys, T. J.; Carlson, R. O. Coherent Light Emission From GaAs Junctions. *Phys. Rev. Lett.* **1962**, *9* (9), 366−368.
(17) Geisz, J. F.; France, R. M.; Schulte, K. L.; Steiner, M. A.; Norman, A. G.; Guthrey, H. L.; Young, M. R.; Song, T.; Moriarty, T. Six-Junction III−V Solar Cells with 47.1% Conversion Efficiency under 143 Suns Concentration. *Nat. Energy* **2020**, *5* (4), 326−335.
(18) Reindl, M.; Weber, J. H.; Huber, D.; Schimpf, C.; Covre Da Silva, S. F.; Portalupi, S. L.; Trotta, R.; Michler, P.; Rastelli, A. Highly Indistinguishable Single Photons from Incoherently Excited Quantum Dots. *Phys. Rev. B* **2019**, *100* (15), No. 155420.
(19) Hornung, F.; Pfister, U.; Bauer, S.; Cyrlyson's, D. R.; Wang, D.; Vijayan, P.; Garcia, A. J.; Covre Da Silva, S. F.; Jetter, M.; Portalupi, S. L.; Rastelli, A.; Michler, P. Highly Indistinguishable Single Photons from Droplet-Etched GaAs Quantum Dots Integrated in Single-Mode Waveguides and Beamsplitters. *Nano Lett.* **2024**, *24* (4), 1184−1190.
(20) Schweickert, L.; Jöns, K. D.; Zeuner, K. D.; Covre Da Silva, S. F.; Huang, H.; Lettner, T.; Reindl, M.; Zichi, J.; Trotta, R.; Rastelli, A.; Zwiller, V. On-Demand Generation of Background-Free Single Photons from a Solid-State Source. *Appl. Phys. Lett.* **2018**, *112* (9), No. 093106.
(21) Lauth, J.; Strupeit, T.; Kornowski, A.; Weller, H. A Transmetalation Route for Colloidal GaAs Nanocrystals and Additional III−V Semiconductor Materials. *Chem. Mater.* **2013**, *25* (8), 1377−1383.
(22) Olshavsky, M. A.; Goldstein, A. N.; Alivisatos, A. P. Organometallic Synthesis of Gallium-Arsenide Crystallites, Exhibiting Quantum Confinement. *J. Am. Chem. Soc.* **1990**, *112* (25), 9438−9439.
(23) Zhang, H.; Dasbiswas, K.; Ludwig, N. B.; Han, G.; Lee, B.; Vaikuntanathan, S.; Talapin, D. V. Stable Colloids in Molten Inorganic Salts. *Nature* **2017**, *542* (7641), 328−331.
(24) Srivastava, V.; Kamysbayev, V.; Hong, L.; Dunietz, E.; Klie, R. F.; Talapin, D. V. Colloidal Chemistry in Molten Salts: Synthesis of Luminescent $In_{1-x}Ga_xP$ and $In_{1-x}Ga_xAs$ Quantum Dots. *J. Am. Chem. Soc.* **2018**, *140* (38), 12144−12151.
(25) Gupta, A.; Ondry, J. C.; Chen, M.; Hudson, M. H.; Coropceanu, I.; Sarma, N. A.; Talapin, D. V. Diffusion-Limited Kinetics of Isovalent Cation Exchange in III−V Nanocrystals Dispersed in Molten Salt Reaction Media. *Nano Lett.* **2022**, *22* (16), 6545−6552.
(26) Gupta, A.; Ondry, J. C.; Lin, K.; Chen, Y.; Hudson, M. H.; Chen, M.; Schaller, R. D.; Rossini, A. J.; Rabani, E.; Talapin, D. V. Composition-Defined Optical Properties and the Direct-to-Indirect Transition in Core−Shell $In_{1-x}Ga_xP$/ZnS Colloidal Quantum Dots. *J. Am. Chem. Soc.* **2023**, *145* (30), 16429−16448.
(27) Ondry, J. C.; Gupta, A.; Zhou, Z.; Chang, J. H.; Talapin, D. V. Synthesis of Ternary and Quaternary Group III-Arsenide Colloidal Quantum Dots via High-Temperature Cation Exchange in Molten Salts: The Importance of Molten Salt Speciation. *ACS Nano* **2024**, *18* (1), 858−873.
(28) Chang, J. H.; Ondry, J. C.; Zangeneh, D.; Zhou, Z.; Gupta, A.; Liu, Y.; Klie, R. F.; Schaller, R. D.; Talapin, D. V. Design of Zn Chalcogenide Shells for Emissive Ga-Rich $In_{1-X}Ga_XAs$ Quantum Dots Synthesized in Molten Salts. *ACS Nano* **2025**, *19* (25), 23096−23104.
(29) Ondry, J. C.; Zhou, Z.; Lin, K.; Gupta, A.; Chang, J. H.; Wu, H.; Jeong, A.; Hammel, B. F.; Wang, D.; Fry, H. C.; Yazdi, S.; Dukovic, G.; Schaller, R. D.; Rabani, E.; Talapin, D. V. Reductive

Pathways in Molten Inorganic Salts Enable Colloidal Synthesis of III-V Semiconductor Nanocrystals. *Science* **2024**, *386* (6720), 401−407.
(30) Yablonovitch, E.; Sandroff, C. J.; Bhat, R.; Gmitter, T. Nearly Ideal Electronic Properties of Sulfide Coated GaAs Surfaces. *Appl. Phys. Lett.* **1987**, *51* (6), 439−441.
(31) Carpenter, M. S.; Melloch, M. R.; Cowans, B. A.; Dardas, Z.; Delgass, W. N. Investigations of Ammonium Sulfide Surface Treatments on GaAs. *Journal of Vacuum Science & Technology B: Microelectronics Processing and Phenomena* **1989**, *7* (4), 845−850.
(32) Sandroff, C. J.; Hegde, M. S.; Chang, C. C. Structure and Stability of Passivating Arsenic Sulfide Phases on GaAs Surfaces. *Journal of Vacuum Science & Technology B: Microelectronics Processing and Phenomena* **1989**, *7* (4), 841−844.
(33) Choi, Y.; Hahm, D.; Bae, W. K.; Lim, J. Heteroepitaxial Chemistry of Zinc Chalcogenides on InP Nanocrystals for Defect-Free Interfaces with Atomic Uniformity. *Nat. Commun.* **2023**, *14* (1), 43.
(34) Hahm, D.; Chang, J. H.; Jeong, B. G.; Park, P.; Kim, J.; Lee, S.; Choi, J.; Kim, W. D.; Rhee, S.; Lim, J.; Lee, D. C.; Lee, C.; Char, K.; Bae, W. K. Design Principle for Bright, Robust, and Color-Pure InP/ZnSe $_x$ S $_{1-x}$ /ZnS Heterostructures. *Chem. Mater.* **2019**, *31* (9), 3476−3484.
(35) Norris, D. J.; Efros, Al. L.; Rosen, M.; Bawendi, M. G. Size Dependence of Exciton Fine Structure in CdSe Quantum Dots. *Phys. Rev. B* **1996**, *53* (24), 16347−16354.
(36) Efros, Al. L.; Rosen, M.; Kuno, M.; Nirmal, M.; Norris, D. J.; Bawendi, M. Band-Edge Exciton in Quantum Dots of Semiconductors with a Degenerate Valence Band: Dark and Bright Exciton States. *Phys. Rev. B* **1996**, *54* (7), 4843−4856.
(37) Biadala, L.; Siebers, B.; Beyazit, Y.; Tessier, M. D.; Dupont, D.; Hens, Z.; Yakovlev, D. R.; Bayer, M. Band-Edge Exciton Fine Structure and Recombination Dynamics in InP/ZnS Colloidal Nanocrystals. *ACS Nano* **2016**, *10* (3), 3356−3364.
(38) Brodu, A.; Ballottin, M. V.; Buhot, J.; Van Harten, E. J.; Dupont, D.; La Porta, A.; Prins, P. T.; Tessier, M. D.; Versteegh, M. A. M.; Zwiller, V.; Bals, S.; Hens, Z.; Rabouw, F. T.; Christianen, P. C. M.; De Mello Donega, C.; Vanmaekelbergh, D. Exciton Fine Structure and Lattice Dynamics in InP/ZnSe Core/Shell Quantum Dots. *ACS Photonics* **2018**, *5* (8), 3353−3362.
(39) Brodu, A.; Chandrasekaran, V.; Scarpelli, L.; Buhot, J.; Masia, F.; Ballottin, M. V.; Severijnen, M.; Tessier, M. D.; Dupont, D.; Rabouw, F. T.; Christianen, P. C. M.; De Mello Donega, C.; Vanmaekelbergh, D.; Langbein, W.; Hens, Z. Fine Structure of Nearly Isotropic Bright Excitons in InP/ZnSe Colloidal Quantum Dots. *J. Phys. Chem. Lett.* **2019**, *10* (18), 5468−5475.
(40) Lin, K.; Coley-O'Rourke, M. J.; Rabani, E. Deep-Learning Atomistic Semi-Empirical Pseudopotential Model for Nanomaterials. *npj Comput. Mater.* **2025**, *11* (1), 381.
(41) Luo, J.-W.; Franceschetti, A.; Zunger, A. Quantum-Size-Induced Electronic Transitions in Quantum Dots: Indirect Band-Gap GaAs. *Phys. Rev. B* **2008**, *78* (3), No. 035306.
(42) Franceschetti, A.; Zunger, A. GaAs Quantum Structures: Comparison between Direct Pseudopotential and Single-Band Truncated-Crystal Calculations. *J. Chem. Phys.* **1996**, *104* (14), 5572−5578.
(43) Williamson, A. J.; Franceschetti, A.; Fu, H.; Wang, L. W.; Zunger, A. Indirect Band Gaps in Quantum Dots Made from Direct-Gap Bulk Materials. *Journal of Elec Materi* **1999**, *28* (5), 414−425.
(44) Díaz, J. G.; Bryant, G. W. Electronic and Optical Fine Structure of GaAs Nanocrystals: The Role of d Orbitals in a Tight-Binding Approach. *Phys. Rev. B* **2006**, *73* (7), No. 075329.
(45) Powell, D.; Migliorato, M. A.; Cullis, A. G. Optimized Tersoff Potential Parameters for Tetrahedrally Bonded III-V Semiconductors. *Phys. Rev. B* **2007**, *75* (11), No. 115202.
(46) Itoh, T.; Nishijima, M.; Ekimov, A. I.; Gourdon, C.; Efros, Al. L.; Rosen, M. Polaron and Exciton-Phonon Complexes in CuCl Nanocrystals. *Phys. Rev. Lett.* **1995**, *74* (9), 1645−1648.
(47) Raymond, S.; Fafard, S.; Charbonneau, S. Temperature Dependence of Ultrasharp Luminescence Lines in Al $_y$ In $_{1-y}$ As/Al $_x$ Ga $_{1-x}$ As Self-Assembled Quantum Dots. *Can. J. Phys.* **1996**, *74* (S1), 216−219.
(48) Mukai, K.; Ohtsuka, N.; Sugawara, M. High Photoluminescence Efficiency of InGaAs/GaAs Quantum Dots Self-Formed by Atomic Layer Epitaxy Technique. *Appl. Phys. Lett.* **1997**, *70* (18), 2416−2418.
(49) Arlett, J.; Yang, F.; Hinzer, K.; Fafard, S.; Feng, Y.; Charbonneau, S.; Leon, R. Temperature Independent Lifetime in InAlAs Quantum Dots. *Journal of Vacuum Science & Technology B: Microelectronics and Nanometer Structures Processing, Measurement, and Phenomena* **1998**, *16* (2), 578−581.

https://doi.org/10.1021/jacs.6c03474
J. Am. Chem. Soc. 2026, 148, 22804−22816